IEEE Photonics Journal
An IEEE Photonics Society Publication

Open Access

Liquid-Crystal Terahertz Quarter-Wave Plate Using Chemical-Vapor-Deposited Graphene Electrodes

Volume 7, Number 6, December 2015

Chan-Shan Yang
Chun Kuo
Chiu-Chun Tang
J. C. Chen
Ru-Pin Pan
Ci-Ling Pan

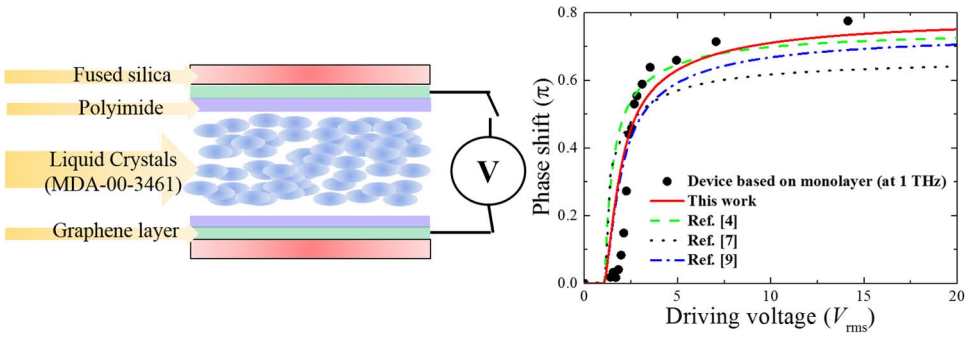

DOI: 10.1109/JPHOT.2015.2504960
1943-0655

Liquid-Crystal Terahertz Quarter-Wave Plate Using Chemical-Vapor-Deposited Graphene Electrodes

Chan-Shan Yang,[1] Chun Kuo,[2] Chiu-Chun Tang,[1] J. C. Chen,[1,4] Ru-Pin Pan,[3] and Ci-Ling Pan[1,4]

[1]Department of Physics, National Tsing Hua University, Hsinchu 30013, Taiwan
[2]Institute of Photonics Technologies, National Tsing Hua University, Hsinchu 30013, Taiwan
[3]Department of Electrophysics, National Chiao Tung University, Hsinchu 30010, Taiwan
[4]Frontier Research Center on Fundamental and Applied Science of Matter, Hsinchu 30013, Taiwan

DOI: 10.1109/JPHOT.2015.2504960

Manuscript received October 16, 2015; revised November 23, 2015; accepted November 24, 2015. Date of publication December 4, 2015; date of current version December 9, 2015. This work was supported in part by the Ministry of Science Technology of Taiwan under Grant 104-2221-E-007-093-MY3, by the Academic Top University Program of the Ministry of Education of Taiwan, and by the U.S. Air Force Office of Scientific Research under Grant FA2386-13-1-4086. Corresponding author: C.-L. Pan (e-mail: clpan@phys.nthu.edu.tw).

Abstract: Quarter-wave operation or a phase shift of more than $\pi/2$, which is approximately ten times greater than that reported in previous works using liquid crystals (LCs) and graphene electrodes, was demonstrated. The device is transparent to the terahertz (THz) wave, and the driving voltage required was as low as approximately 2.2 V (rms), which is also unprecedented. Experimental results supported a theoretical formalism adapted for LC cells with THz wavelength-scale thickness. The scattering rate, DC mobility, and carrier mean free path of bilayer graphene were also determined using THz spectroscopic techniques; the parameters were inferior to those of monolayer graphene. This observation can be attributed to the higher density of charged impurities in the bilayer graphene. The device performances of LC phase shifters using monolayer and bilayer graphene as electrodes were essentially identical.

Index Terms: Far infrared or terahertz, phase shift, liquid crystals, nanomaterials, liquid-crystal devices, birefringence, spectroscopy.

1. Introduction

Over the past few decades, remarkable progress has been made in terahertz (THz) technology, which has applications in high-data-rate wireless communications [1], biomedicine, 3-D imaging, tomography, and material characterization [2]. Functional quasi-optical components, therefore, are in high demand. In particular, numerous tunable THz devices employing liquid crystals (LCs), such as phase shifters [3]–[10], filters [11], phase gratings [12], and polarizers [13], have been developed. Early studies in the field of tunable THz devices have mostly focused on magnetically tuned components [3]. Although these devices can fulfill their intended functions, their bulky and heavy design poses obvious problems. Electrically tuned components with a compact size are expected to aid in overcoming this problem [4]. Furthermore, indium tin oxide (ITO) films, which are widely used as transparent electrodes in LC devices operating in the visible wavelength range, are opaque in the THz frequency range [14], [15]. Therefore, the lack of

transparent electrodes in the THz frequency region continues to pose a challenge in the field of electrically tuned components based on LCs, leading to tunable THz devices having low transmittance and requiring a high driving voltage. In 2011, a self-polarizing THz phase shifter capable of a phase shift of $\pi/3$ at 2 THz with high transmittance was demonstrated using a subwavelength metallic grating. However, the operating voltage, approximately 130 V (rms), was high [5]. Recently, we found that ITO nanowhiskers (NWhs) not only exhibit outstanding transmittance in the terahertz region but show high DC mobility and conductivity comparable to those of ITO thin films as well [14]–[16]. Furthermore, we demonstrated quarter-wave plates $(\pi/2)$ operating at 1.0 THz; they contained ITO NWhs, used as transparent electrodes [8], [9], and also as an alignment layer [9]. The quarter-wave plates exhibited the desirable characteristics of high transmittance (approximately 78%) and a low operation voltage (5.66 V (rms)) and were compatible with complementary-metal-oxide-semiconductor (CMOS) and thin-film-transistor (TFT) technologies.

Graphene, a kind of two-dimensional materials, is characterized by high conductivity, mobility, and chemical stability. In view of its optoelectronic applications, numerous studies have examined the electrical transport properties of graphene layers such as hot electron transport [17], charged-impurity-induced scattering [18], and substrate-induced effects [19]. Moreover, graphene shows high transmittance not only in the visible [20], [21] but the THz frequency range as well [7], [10], [20]. Such unique properties make graphene an attractive material for optoelectronic devices in the THz frequency range. In a previous study, a THz phase shifter based on transparent graphene conductors was demonstrated and achieved a maximal phase shift of 10.8° at an operating voltage of 5 V [7]. Subsequently, Sasaki *et al*. presented a polarization-independent THz phase controller, containing a randomly aligned LC cell with graphene electrodes [10]. That could achieve a maximal phase shift of 0.10 rad. However, reported phase shifts in these works are too small for most THz applications [7], [10]. Furthermore, theoretical models used cannot accurately describe the behavior of phase shifters operating at low bias voltages [7].

In this study, by applying THz time-domain spectroscopy (THz-TDS), the THz transmittance and complex conductivities of monolayer and bilayer graphene sheets were thoroughly examined in the frequency range of 0.3–1.4 THz. The electrical properties of the two types of graphene sheets, such as scattering rate, DC mobility, and carrier mean free path, were determined and compared to that of ITO NWhs. Monolayer and bilayer graphene were successfully used in electrically tunable LC phase shifters as transparent electrode. Quarter-wave operation was demonstrated. The voltage- and frequency-dependent characteristics of the THz phase shifters are presented. The experimental results are in good agreements with theoretical predictions made by considering the minimum free energy condition and correction of LC thickness in the scale of THz wavelengths.

2. Theory and Experiment

2.1. Theoretical Analysis

The theoretical model of the phase shifter is based on the electro-optical distortion model for of a LC cell of thickness d, traversed by THz waves. In the absence of an external field, LC molecules are assumed to be initially in a stable state and oriented parallel to the rubbed direction set as the x-direction in this work. This implies that the director of orientation $\theta(z)$ must satisfy the boundary condition, $\theta(0) = \theta(d) = 0$, on internal surfaces of substrates for the LC cell. Assuming the maximum tilt angle, $\theta_{\max}$, occurs at the center of the cell $z = d/2$, the dependence of $\theta_{\max}$ and on the strength of the applied voltage can be derived [8], [9], [22]. When the applied voltage exceeds the threshold voltage, $V_{\text{th}} = E_{\text{th}}L = \pi[k_1/(\varepsilon_0 \cdot \Delta\varepsilon)]^{1/2}L/d$, the LC molecules are reoriented toward the external field, where E_{th} is the corresponding threshold electric field, $\varepsilon_0 = 8.854 \times 10^{-12}\,\text{F}\cdot\text{m}^{-1}$, $\Delta\varepsilon = 11.2$, $k_1 = 12.6 \times 10^{-12}$ N, L, and d are the free-space permittivity, dielectric anisotropy, splay elastic constants, distance between two electrodes, and

thickness of the LCs layer, respectively. After calculating θ_{max} at every applied voltage, the distribution of director tilt angle $\theta(z)$ at every position z can then be obtained [22]. The effective birefringence, $\Delta n_{eff}(z)$, experienced by the THz wave passing through the LC cell can be written as, $[\cos^2\theta(z)/n_o^2 + \sin^2\theta(z)/n_e^2]^{-1/2} - n_o$, where n_e and n_o are extraordinary and ordinary indices of refraction of the LC, respectively [8], [9]. Finally, the phase shift is given by

$$\varphi = \int_0^d \frac{2\pi f}{c_0}\Delta n_{eff}(z)dz = \int_0^d \frac{2\pi f}{c_0}\left[\left(\frac{\cos^2\theta}{n_o^2} + \frac{\sin^2\theta}{n_e^2}\right)^{-1/2} - n_o\right]dz \quad (1)$$

where f and c_0 are the frequency and speed of propagation of the THz wave in vacuum, respectively. The aforementioned model is ordinarily used for a thin LC cell (approximately 20 μm or less) operating in the visible frequency range. However, the LC THz phase shifter is much thicker due to the operation wavelength. In this study, the thickness of the LC layer was approximately 0.55 mm. In such a thick sample, LC molecules more than a few tens of microns away from the cell walls will not be perfectly parallel to the rubbed direction in the absence of the externally applied electric field. On the other hand, when applying a driving voltage, almost all the LC molecules will be easily orientated in the direction which is parallel to the external field. In order to describe this behavior, we first need to achieve the e-ray mode without bias for a thick LC cell. Secondly, after applying a sufficiently high voltage, we can get the o-ray mode for the cell. From the measured phase difference of these two modes, the maximum relative phase retardation, $\phi(V_{max})$, can be determined. Then, by considering the total relative phase shift in the ideal case, $2\pi f(n_e - n_o)d/c$, with the experimentally measured relative phase shifts for the thick LC cells operating in the o-ray mode (cell biased at $V_{max} = 70$ V) and the e-ray mode (cell without bias), we can define a correction factor,

$$\alpha = \frac{2\pi f(n_e - n_o)d/c_0}{\phi(V_{max})} \quad (2)$$

to compensate for effects of the thick LC cell, Finally, the effective phase shift can be expressed as $\alpha \times \phi$. For thin LC cell $\alpha = 1$, we have the case of ordinary thin LC cells. For the case of $\alpha > 1$, the LC molecules in the middle of cell are not aligned well along the rubbed direction because of the weak ability of alignment in a thick LC device. The total relative phase retardation observed experimentally is smaller than theoretical one.

2.2. Preparation and Characterization of Graphene

Graphene was grown by chemical vapor deposition and transferred to fused silica substrates. Details of the growth parameters and transfer procedures can be found in our previous publication [23]. Bilayer graphene samples were obtained by repeating the transfer processes twice. Subsequently, Cr/Au (5 nm/20 nm) gate electrodes were deposited to establish Ohmic contact with the graphene. Previously, we have demonstrated this Ohmic contact and described the process in detail [18], [23]. The contact resistance of graphene-Cr/Au contacts for is around $10^3 \sim 10^6$ Ω μm [24]. We used Raman spectroscopy (632 nm wavelength) to examine the quality of monolayer graphene transferred onto the silica substrates. The G and 2D peaks shown in the inset of Fig. 1(a) are at approximately 1580 and 2650 cm^{-1}, respectively. The intensity ratio I_{2D}/I_G of approximately 1.8 indicated that the quality of monolayer graphene on the fused silica substrate was comparable to that reported previously [23]. To obtain the complex THz conductivities and transmission coefficients of the graphene samples, we employed THz-TDS based on photoconductive antenna and laser-induced air plasma, as described in a previous study [15]. During measurements, both types of THz-TDS systems were purged with nitrogen at a relative humidity of 4.5 $\pm$ 0.5%.

In the thin-film approximation, the complex transmission coefficient t and complex conductivity $(\sigma(\omega))$ of a graphene sample were related through, $t = (1 + n_{sub})/(1 + n_{sub} + Z_0\sigma(\omega)D)$, where

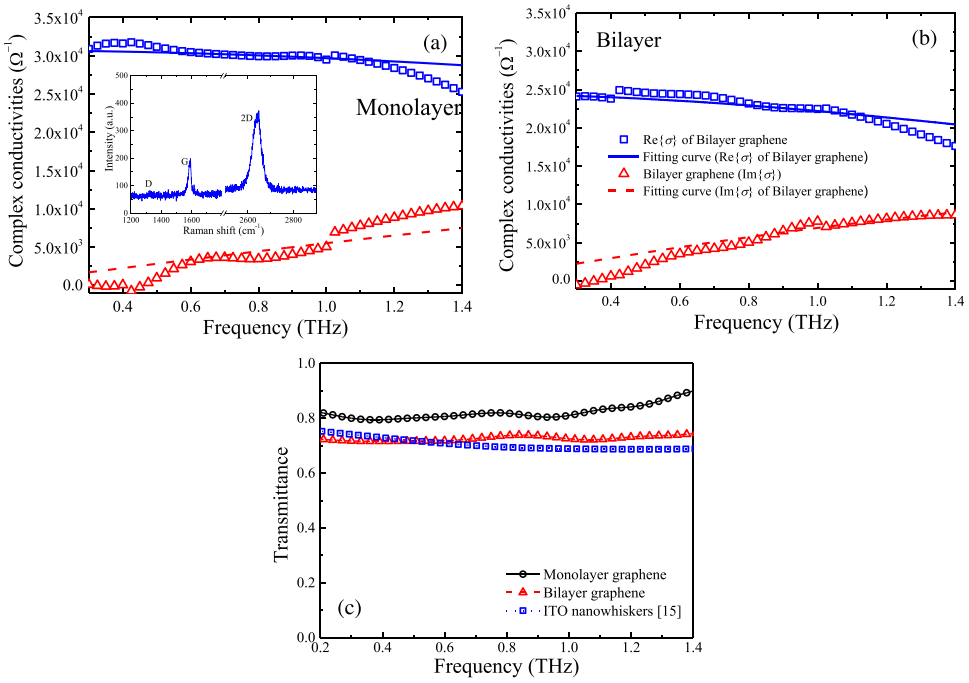

Fig. 1. Real (blue squares) and imaginary (red triangles) parts of the conductivity of (a) monolayer and (b) bilayer graphene sheets. The solid and dashed lines indicate the fitting results yielded using the Drude model. (c) THz transmittance of monolayer graphene, bilayer graphene, and ITO nanowhiskers, respectively. Table 1 lists the parameters obtained.

Z_0 is the impedance of free space, n_{sub} is the refractive index of the substrate, and D is the graphene sheet thickness [25]. In this work, the thicknesses of monolayer and bilayer graphene are estimated as 0.3 nm, and 0.6 nm, respectively. We fit experimental data to the Drude free-electron conductivity, i.e., $\sigma(\omega) = \sigma_0/(1 + i\omega\tau)$, where σ_0 and τ are the DC conductivity and scattering time of graphene, respectively. The complex THz conductivities of the monolayer and bilayer graphene thus obtained are shown in Fig. 1(a) and (b), respectively. From which, we can calculate the mobility (μ) and plasma frequency (ω_p) of the graphene samples using the expressions $\mu = e\tau/m^*$ and $\omega_p^2 = \sigma_0/(\varepsilon_0\tau)$ [14], respectively, where e, m^*, and ε_0 are the electron charge, effective electron mass of single-layer graphene [26], and vacuum permittivity, in this order. In the frequency range of 0.2~1.4 THz, the transmittance of monolayer graphene, bilayer graphene, and ITO nanowhiskers are approximately frequency-independent with average values of 0.82 ± 0.03, 0.73 ± 0.01, and 0.70 ± 0.01, respectively (see Fig. 1(c)).

The optical and electrical characteristics of monolayer and bilayer graphene sheets, deduced from THz-TDS are summarized and compared to those of ITO NWhs in Table 1. For example, the carrier scattering times of mono- and bi-layer graphene samples were 30 and 50 fs while the corresponding mobilities were 4400 and 2000 $cm^2/V \cdot s$, respectively. We estimated the inelastic mean free path (MFP), L_M, associated with the scattering between electrons by using $L_M = V_F\tau$, where V_F and τ are the Fermi velocity and carrier scattering time [27], respectively. The parameter V_F was calculated for the monolayer graphene as 1.77×10^6 m/s, close to the 1.1×10^6 m/s reported previously [28], and for the bilayer graphene as 0.58×10^6 m/s; the corresponding MFPs were 53.2 and 29.1 nm, respectively. The difference can be attributed to the effect of higher charged impurity density in the bilayer graphene. Thus, the mobility and MFP were considerably lower in the bilayer sample. The conductivities of the two samples, however, are comparable. Notably, the transmittances of devices containing the monolayer and bilayer graphene in the THz frequency range were very high, approximately 82% and 73%, respectively, comparable or somewhat higher than ITO NWhs studied previously and employed as

TABLE 1

Electrical and optical parameters of monolayer, bilayer graphene sheets, and indium-tin-oxide (ITO) nanowhiskers (NWhs)

ω_p(rad·Hz)	τ(fs)	σ_0 (Ω^{-1})	μ (cm^2/Vs)	Transmittance (0.2~1.4 THz)
Monolayer graphene				
3.42×10^{15}	30	3.07×10^{4}	4400	82 ± 3 %
Bilayer graphene				
2.35×10^{15}	50	2.44×10^{4}	2000	73 ± 1%
ITO NWhs (long NWhs ≈ 1 μm) [15]				
8.53×10^{14}	13.2	221	20.3	70 ± 1%

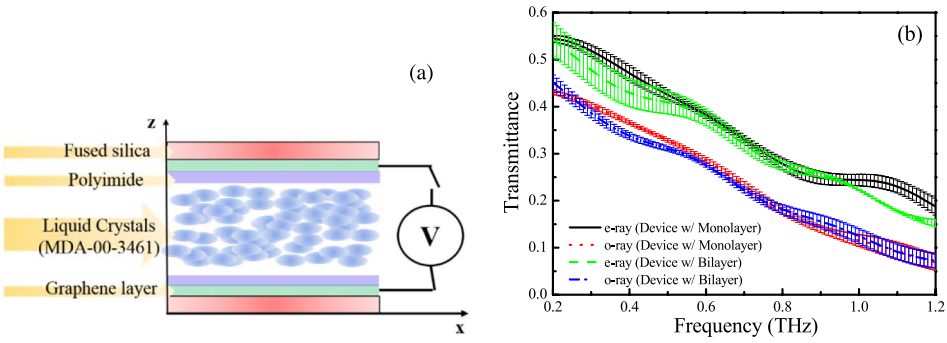

Fig. 2. (a) Schematic diagram of an LC THz phase shifter containing transparent graphene electrodes. (b) THz transmittance of the phase shifters with monolayer and bilayer graphene as transparent electrodes for e-rays and o-rays.

transparent electrodes in the THz frequency range [15]. On the other hand, the DC conductivity ($\sim10^4$ versus $\sim10^2$ Ω^{-1}) and mobility ($\sim10^3$ versus $\sim10^1$ cm^2/Vs) of graphene sheets are significantly higher than those of ITO NWhs.

3. Results and Analysis

Phase shifters were constructed by sandwiching a nematic LC (MDA-00-3461 by Merck) layer between two fused silica substrates with transferred graphene and spin-coated polyimide layers, which were used as electrodes and alignment layers, respectively. Fig. 2(a) depicts the configuration of a phase shifter; the thickness of the substrate and an LC layer was approximately 1.033 and 0.55 mm for the cell with monolayer and bilayer graphene, respectively. The extraordinary and ordinary refractive indices of MDA-00-3461 are approximately constant and equal to $n_e = 1.74$ and $n_o = 1.54$ at 25 °C from 0.3 to 1.4 THz [29]. The cells were biased with sinusoidal signals at 1 kHz. The photoconductive antenna-based THz-TDS, described in our previous studies, was used to characterize the characteristics of devices in the frequency range between 200 GHz and 1.4 THz [14], [15]. Fig. 2(b) plots the frequency-dependent transmittances of devices with the monolayer and bilayer graphene substrates for extraordinary (e-ray) and ordinary rays (o-ray). In general, for the devices with monolayer and bilayer graphene, the e-ray transmittance was always higher than the o-ray transmittance, and it decreased from 55% to 20% between frequencies of 0.2 and 1.2 THz. The loss is mainly contributed by the LC itself and the fused silica substrates.

Fig. 3 compares the experimentally observed THz phase shifts with the current theoretical model and those employed in previous studies [4], [7], [9]. In order to describe the difference between the experimental data and the theoretical results quantitatively and check which theoretical method is better, we divide the range of driving voltage of $0 \sim 20$ V_{rms} into 20 points, and define an error function as $\eta = \Sigma|P_{i,\text{theo}} - P_{i,\text{exp}}|$, where i equals $1, 2, \ldots, 20$. The parameters,

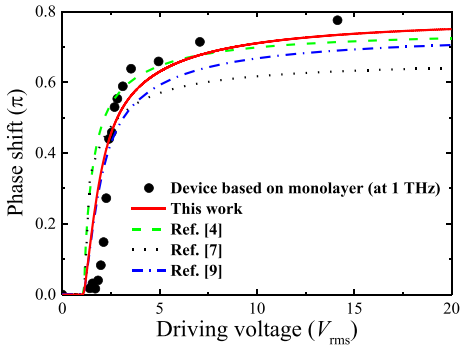

Fig. 3. Comparison of the experimentally measured phase shift as a function of the driving voltage and different theoretical models.

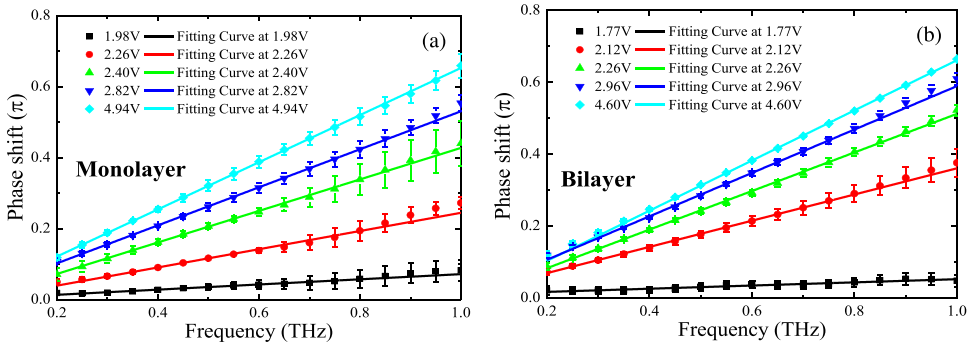

Fig. 4. Phase shift as a function of the frequency for phase shifters containing (a) monolayer and (b) bilayer graphene electrodes at several driving voltages.

$P_{i,\text{theo}}$ and $P_{i,\text{exp}}$, represent the theoretical and experimental phase shift when a bias voltage, V_i, was applied. Employing the theoretical method described in [4], [7], [9], and this work, η were found to be 2.75, 2.89, 1.97, and 1.79, respectively. This clearly demonstrated that the theoretical formulism presented in this work fits the experimental data better. For the phase shifters with monolayer and bilayer graphene as transparent electrodes, $\alpha \approx 1.064$, corresponding to the case of weak LC alignment in thick THz LC cells.

In Fig. 4, we plot the phase shifts as a function of frequency from 0.2 to 1.0 THz for several applied voltages. A linear frequency dependence can be seen, as expected.

In Fig. 5, the phase shift is shown as a function of the driving voltage. The fitting curves agree with the theoretical predictions according to (1) and (2). The experimental results of phase shifters are in good agreement with the theoretical predictions. The operating voltage for achieving a phase shift of $\pi/2$ at 1.0 THz of the monolayer and bilayer graphene-based phase shifters are about 2.6 and 2.2 V (rms), respectively. These are substantially lower than that reported in our previous work using ITO NWhs as transparent electrodes, i. e., 5.66 V (rms). We have tentatively attributed this observation to the superior electrical properties, e.g., the DC conductivity ($\sim 10^4$ versus $\sim 10^2\ \Omega^{-1}$) and mobility ($\sim 10^3$ versus $\sim 10^1\ \text{cm}^2/\text{Vs}$) of graphene versus that of ITO NWhs. Theoretically, the voltage drop is proportional to the impedance, which is the inverse of DC conductivity. Therefore, if conductivity of the electrode material is higher, we should expect lower driving voltage for the device. Furthermore, the average transmittance of the two LC cells is as high as 38.1% and 36.6%, respectively.

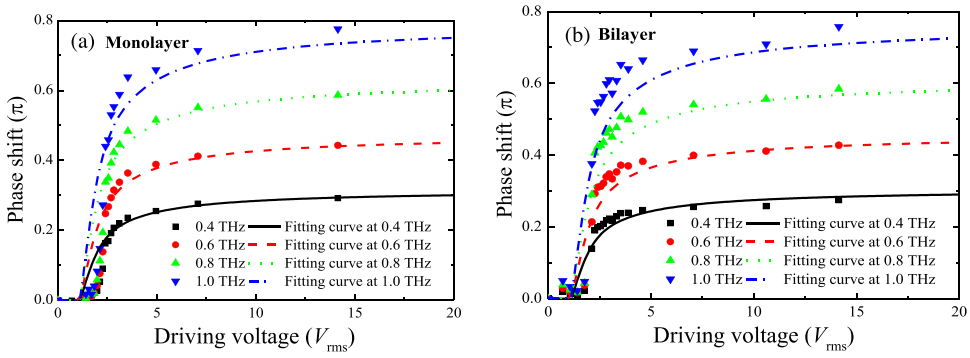

Fig. 5. Plots of phase shift versus driving voltage for phase shifters with (a) monolayer and (b) bilayer graphene electrodes.

4. Conclusion

The mono- and bi-layer graphene sheets, which exhibit outstanding properties such as high transparency in the far-infrared and high electrical conductivity, were determined using THz-TDS. The complex conductivities of the graphene samples were fitted well with the Drude free-electron model. The electrical properties of the samples, such as the plasma frequency (ω_p), scattering time (τ), DC mobility (μ), and DC conductivity (σ_0), were obtained for both samples. The mean free paths (MFPs) of monolayer and bilayer graphene were found to be 53.2 and 29.1 nm, respectively. These values can be attributed to the presence of a higher density of charged impurities in the bilayer graphene. As a result, the mobility and MFP of the graphene bilayer were considerably lower. Performance of phase shifters using either type of graphene samples is compared with that using ITO NWhs as transparent electrodes. The monolayer graphene was shown to exhibit high transmittance (80%), DC conductivity $(\sim 3 \times 10^4\ \Omega^{-1})$, and mobility $(\sim 4000\ \text{cm}^2/\text{Vs})$. Furthermore, quarter-wave operation or a phase shift of more than $\pi/2$, approximately 10 times greater than the phase shift achieved previously in graphene-based devices, was demonstrated. The driving voltage required was as low as approximately 2.2 V (rms), which is also a new record. The experimental results supported a theoretical formalism adapted for super-thick THz LC devices.

Acknowledgment

The authors would like to thank Dr. T.-T. Tang for useful discussions.

References

[1] J.-W. Shi, C. B. Huang, and C.-L. Pan, "Millimeter-wave photonic wireless links for very-high data rate communication," *NPG Asia Mater.*, vol. 3, no. 4, pp. 41–48, Apr. 2011.
[2] X.-C. Zhang and J. Xu, *Introduction to THz Wave Photonics*. New York, NY, USA: Springer-Verlag, 2010.
[3] C.-Y. Chen, C.-F. Hsieh, Y.-F. Lin, R.-P. Pan, and C.-L. Pan, "Magnetically tunable room-temperature 2π liquid crystal terahertz phase shifter," *Opt. Exp.*, vol. 12, no. 12, pp. 2630–2635, Jun. 2004.
[4] H.-Y. Wu, C.-F. Hsieh, T.-T. Tang, R.-P. Pan, and C.-L. Pan, "Electrically tunable room-temperature 2π liquid crystal terahertz phase shifter," *IEEE Photon. Technol. Lett.*, vol. 18, no. 14, pp. 1488–1490, Jul. 2006.
[5] X.-W. Lin *et al.*, "Self-polarizing terahertz liquid crystal phase shifter," *AIP Adv.*, vol. 1, no. 3, Sep. 2011, Art. ID 032133.
[6] K. Altmann *et al.*, "Polymer stabilized liquid crystal phase shifter for terahertz waves," *Opt. Exp.*, vol. 21, no. 10, pp. 12395–12400, May 2013.
[7] Y. Wu *et al.*, "Graphene/liquid crystal based terahertz phase shifters," *Opt. Exp.*, vol. 21, no. 18, pp. 21395–21402, Sep. 2013.
[8] C.-S. Yang *et al.*, "Voltage-controlled liquid-crystal terahertz phase shifter with indium-tin-oxide nanowhiskers as transparent electrodes," *Opt. Lett.*, vol. 39, no. 8, pp. 2511–2513, Apr. 2014.
[9] C.-S. Yang, T.-T. Tang, R.-P. Pan, P. Yu, and C.-L. Pan, "Liquid crystal terahertz phase shifters with functional indium-tin-oxide nanostructure for biasing and alignment," *Appl. Phys. Lett.*, vol. 104, no. 14, Apr. 2014, Art. ID 141106.

[10] T. Sasaki, K. Noda, N. Kawatsuki, and H. Ono, "Universal polarization terahertz phase controllers using randomly aligned liquid crystal cells with graphene electrodes," *Opt. Lett.*, vol. 40, no. 7, pp. 1544–1547, Apr. 2015.
[11] Y.-J. Chiang, C.-S. Yang, Y.-H. Yang, C.-L. Pan, and T.-J. Yen, "An ultrabroad terahertz bandpass filter based on multiple-resonance excitation of a composite metamaterial," *Appl. Phys. Lett.*, vol. 99, no. 19, Nov. 2011, Art. ID 191909.
[12] I. Chatzakis *et al.*, "One- and two-dimensional photo-imprinted diffraction gratings for manipulating terahertz waves," *Appl. Phys. Lett.*, vol. 103, no. 4, Jul. 2013, Art. ID 043101.
[13] C.-F. Hsieh, Y.-C. Lai, R.-P. Pan, and C.-L. Pan, "Polarizing terahertz waves with nematic liquid crystals," *Opt. Lett.*, vol. 33, no. 11, pp. 1174–1176, Jun. 2008.
[14] C.-S. Yang *et al.*, "Non-Drude behavior in indium-tin-oxide nanowhiskers and thin films investigated by transmission and reflection THz time-domain spectroscopy," *IEEE J. Quantum Electron.*, vol. 49, no. 8, pp. 677–690, Aug. 2013.
[15] C.-S. Yang, C.-M. Chang, P.-H. Chen, P. Yu, and C.-L. Pan, "Broadband terahertz conductivity and optical transmission of Indium-Tin-Oxide (ITO) nanomaterials," *Opt. Exp.*, vol. 21, no. 14, pp. 16670–16682, Jul. 2013.
[16] C.-S. Yang *et al.*, "THz conductivities of indium-tin-oxide nanowhiskers as a graded-refractive-index structure," *Opt. Exp.*, vol. 20, no. S4, pp. A441–A451, Jul. 2012.
[17] W.-K. Tse, E. H. Hwang, and S. D. Sarma, "Ballistic hot electron transport in graphene," *Appl. Phys. Lett.*, vol. 93, no. 2, Jul. 2008, Art. ID 023128.
[18] M.-Y. Li *et al.*, "Charged impurity-induced scatterings in chemical vapor deposited graphene," *J. Appl. Phys.*, vol. 114, no. 23, Dec. 2013, Art. ID 233703.
[19] W. Gannett *et al.*, "Boron nitride substrates for high mobility chemical vapor deposited graphene," *Appl. Phys. Lett.*, vol. 98, no. 24, Jun. 2011, Art. ID 242105.
[20] J. M. Dawlaty *et al.*, "Measurement of the optical absorption spectra of epitaxial graphene from terahertz to visible," *Appl. Phys. Lett.*, vol. 93, no. 13, Sep. 2008, Art. ID 131905.
[21] P. Blake *et al.*, "Graphene-based liquid crystal device," *Nano Lett.*, vol. 8, no. 6, pp. 1704–1708, Jun. 2008.
[22] P. Yeh and C. Gu, *Optics of Liquid Crystal Displays*. Hoboken, NJ, USA: Wiley, 2009.
[23] C.-C. Tang, M.-Y. Li, L. J. Li, C. C. Chi, and J. C. Chen, "Characteristics of a sensitive micro-Hall probe fabricated on chemical vapor deposited graphene over the temperature range from liquid-helium to room temperature," *Appl. Phys. Lett.*, vol. 99, no. 11, Sep. 2011, Art. ID 112107.
[24] J. S. Moon *et al.*, "Ultra-low resistance Ohmic contacts in graphene field effect transistors," *Appl. Phys. Lett.*, vol. 100, no. 20, May 2012, Art. ID 203512.
[25] G. Gruener, *Millimeter-Wave Spectroscopy of Solids*. Berlin, Germany: Springer-Verlag, 1997.
[26] E. Tiras *et al.*, "Effective mass of electron in monolayer graphene: Electron-phonon interaction," *J. Appl. Phys.*, vol. 113, no. 4, Jan. 2013, Art. ID 043708.
[27] Q. Li and S. D. Sarma, "Finite temperature inelastic mean free path and quasiparticle lifetime in graphene," *Phys. Rev. B, Condens. Matter Mater. Phys.*, vol. 87, no. 8, Feb. 2013, Art. ID 085406.
[28] J. Y. Kim *et al.*, "Far-infrared study of substrate-effect on large scale graphene," *Appl. Phys. Lett.*, vol. 98, no. 20, May 2011, Art. ID 201907.
[29] C.-P. Ku, C.-C. Shih, C.-J. Lin, R.-P. Pan, and C.-L. Pan, "THz optical constants of the liquid crystal MDA-00-3461," *Mol. Cryst. Liquid Cryst.*, vol. 541, no. 1, pp. 303–308, Jun. 2011.